Mapping Grid Inertia: A Deterministic Graph-Theoretic Framework for Coherent Partitioning and RCOI Identification

ALEXANDER SANCHEZ-OCAMPO[1], MARIO R. ARRIETA PATERNINA[2], JUAN M. RAMIREZ[1,*], ARTURO DIAZ PEREZ[1]

[1]Centre for Research and Advanced Studies,
Guadalajara, 45019, JAL,
MEXICO

[2]National Autonomous University of Mexico,
Mexico City, 04510, MEX,
MEXICO

Abstract: - Integrating spectral centrality with an enhanced label propagation technique, a graph-based methodology for regional frequency assessment is presented in this paper. The method identifies two quantities: the system centre of inertia and the coherent electrical communities from which regional centres of inertia are then derived. Generator bus locations and branch admittances are analysed to begin the approach, after which the network is partitioned into clusters that exhibit consistent dynamic behaviour. From these clusters, regional centres of inertia (RCOIs) are identified. Optimisation of the placement of phasor measurement units (PMUs) for monitoring is carried out by the framework. Through validation using the NETS-NYPS benchmark system, appropriate performance is demonstrated by the results. Confirmation of the precision of the identified regional centres of inertia is provided by the RMSE between the analytical COI frequency and the RCOI frequency. Real-time frequency tracking is improved when PMUs are deployed and effective network clustering methods are used, and grid stability is thereby helped to be maintained.

Key-words: - Centre of inertia, Community detection, Graph analysis, Frequency monitoring, Structural analysis.

Received: May 11, 2026. Revised: June 5, 2026. Accepted: August 7, 2026. Published: November 1, 2026.

Nomenclature

Symbol	Description
$\mathbf{A}$	Adjacency matrix
$\mathbf{c}_e$	Spectral centrality vector
c_k	Cohesion metric for the *k-th* cluster
$\mathbf{D}$	Degree matrix
$d_{\min}$	Minimum admittance threshold for label propagation
E	Set of edges
f_{COI_α}	Analytical COI frequency for area α
f_{RCOI_α}	Measured frequency at RCOI for area α
$G(V,E)$	Undirected graph of the power system
H	Machine inertia constant
$\mathbf{L}$	Laplacian matrix
L_i	Label of the *i-th* node
m	Number of edges
n	Number of vertices
n_g	Number of generators
$N(i)$	Neighbouring nodes of the *i-th* vertex
S_i	Subgraph of the *i-th* community
ss	Silhouette score
V	Set of vertices
$\mathbf{W}$	Weighted adjacency matrix
$\mathbf{Y}$	Complex admittance matrix
y_{ij}	Element of $\mathbf{Y}$
λ_d	Dominant eigenvalue of $\mathbf{L}$
$\mathbf{\Lambda}$	Diagonal matrix of eigenvalues
ω	Angular velocity
ω_{COI}	COI angular velocity
$\mathbf{\Phi}$	Matrix of right eigenvectors
$\mathbf{\Phi}_d$	Dominant eigenvector
$\mathbf{\Psi}$	Matrix of left eigenvectors

1. Introduction

Frequency stability in modern power systems is challenged by the integration of variable renewable energy sources and changing consumption patterns [1]. Regional frequency representation is widely acknowledged as central. Its computation, however, is made difficult by three primary factors: (*i*) constraints in the available measurement data, (*ii*) communication delays, and (*iii*) the intrinsic complexity of inertia estimation [2]. An important obstacle is presented to conventional approaches by the identification of the centre of inertia (COI), which is paramount to stability assessment [6]. Interarea oscillation analysis [3], ARMAX modelling [4], and swing equation-based methods [5] are all affected. Ubiquitous coverage by phasor measurement units (PMUs) is assumed by many conventional methods, a practice which is impractical and costly [7]. Rate-of-change-of-frequency (RoCoF) measurements are compromised by incorrect COI identification [8].

For network partitioning, clustering methods are widely used. Centroid-based approaches, such as K-means, are known to be sensitive to initialisation [9,10]. Inherent limitations are present in affinity propagation [11], routine analysis [12], and DBSCAN [13]. Promise is shown by hierarchical clustering [14]; however, robust validation benchmarks are lacking, particularly for the determination of the optimal number of clusters [15,16].

As an alternative to graph-based methods, spectral clustering and label propagation are regarded [17, 18]. Random initialisation is commonly used in these methods, and non-deterministic outcomes are produced as a result, which are unsuitable for real-time control. In this paper, a deterministic approach is proposed, one in which (*i*) spectral graph analysis, (*ii*) electrical constraints, (*iii*) admittance matrices, and (*iv*) generator locations are integrated. Through this integration, RCOIs are identified without requiring inertia constants.

1.1 Problem Statement

Accurate RCOI frequency estimation is considered essential for power system stability control [19]. Three primary obstacles are recognised. (*i*) Complete measurement coverage from all generators is unattainable, and inertia contributions are subject to variation over time. (*ii*) Communication delays are shown to hinder real-time evaluation, just as limited PMU deployment restricts network visibility [20]. (*iii*) Multiple COIs are displayed by modern interconnected systems. Inertia assessment, meanwhile, is rendered more complex by non-synchronous generation. Under such conditions, only inconsistent results are yielded by existing clustering techniques [21-24].

1.2 Novelty and Contribution

For power system frequency assessment, a deterministic hybrid framework is proposed in this paper, one in which the principles of graph theory and electrical physics are brought together.

The contributions presented herein are threefold, each addressing a distinct challenge in robust, real-time frequency monitoring.

Deterministic label propagation with electrical constraints

The traditional label propagation algorithm (LPA) is known to be stochastic in nature [25-30]. Our proposal represents a variation: labels are initialised at the generator buses, nodes are enriched with clear physical meaning, and propagation is carried out through admittance-weighted increments, governed by a minimum electrical distance threshold dmin. Label diffusion is performed strictly in accordance with the grid's inherent electrical connectivity. As a result, robust, electrically cohesive communities are produced, entirely free of randomness.

Regional centre of inertia identification via eigenvalue dominance of the Laplacian matrix (EDLM)

To identify regional centres of inertia (RCOIs) within each cluster, spectral centrality is employed. In the Laplacian matrix, derived directly from the admittance matrix, the bus with the highest spectral centrality is identified as the node with the strongest informational connectivity; consequently, it is taken as the RCOI. Thus, a purely topology‑driven criterion is established, requiring no prior knowledge of inertia constants.

Physics-based validation framework

The validity of the clustering outcome is assessed by means of the root-mean-square error (RMSE) computed between the analytical COI frequency [31-34] and the frequency measured at the designated RCOI. Through this comparison, a quantitative and physically meaningful criterion is provided, one that links the structural clustering of the network to its dynamic behaviour. In this manner, the gap between topological abstraction and physical reality is bridged. When these three elements are combined, reproducible results are enabled, and real-time applications within power networks with changing inertia and distributed generation could be served by them.

The relationship between this work and the previous research on PMU allocation and spectral clustering

[35] is as follows. The allocation of phasor measurement units for the estimation of the system-wide inertial frequency response is the subject of Reference [35]. The sensor placement objective is determined by the observability of the inertial response. A distinct and prior question is addressed by the current paper, namely the identification of a representative bus within each electrically coherent area, along with the partitioning of the network. Thus, the two pieces address distinct issues.

Different instruments are also used. In Reference [35], spectral clustering is employed as an allocation tool. The current paper, by contrast, is a deterministic partitioning procedure based on electrically constrained label propagation. Besides, the paper introduces a distinct criterion, EDLM, for designating the representative bus. PMU placement is only mentioned in the present paper as a downstream application of RCOI identification, and not as a standalone contribution. Therefore, the novelty asserted in this paper is derived from the determinism of the partitioning, the physics-based validation of the resulting clusters against the analytical COI frequency, and the elimination of inertia data from the identification step.

2. Fundamentals

2.1 Power System Graph Modelling

A power system is represented as an undirected graph $G = (V, E)$, where $V = \{v_1, \dots, v_n\}$ are buses and $E = \{e_1, \dots, e_m\}$ are transmission lines [23]. The adjacency matrix $\mathbf{A} \in \mathbb{R}^{n \times n}$ is binary and symmetric:

$$A_{ij} = \begin{cases} 1 & \text{if } (v_i, v_j) \in E,\ i \neq j \\ 0 & \text{otherwise} \end{cases} \quad (1)$$

The degree matrix $\mathbf{D} \in \mathbb{R}^{n \times n}$ is diagonal with $D_{ii} = \sum_j A_{ij}$. The Laplacian matrix becomes:

$$\mathbf{L} = \mathbf{D} - \mathbf{A} \quad (2)$$

It should be noted that spectral clustering has been used elsewhere in the power system literature, including by the present authors in [35], as a tool for PMU allocation. The use of the Laplacian spectrum in the present paper is different in purpose: it is used to rank buses within an already identified community, and not to partition the network.

2.2 Label Propagation Algorithm

In LPA, each node initially holds a unique label. Nodes iteratively adopt the most frequent label among neighbours [25]. The update rule is:

$$L_i(q+1) = \arg\max_L \sum_{v_j \in N(i)} \mathbf{1}(L_j(q) = L) \quad (3)$$

where $N(i)$ is the neighbourhood of v_i. The process terminates when labels stabilise:

$$L_i(q+1) = L_i(q), \forall i \in V \quad (4)$$

Nodes sharing the same label form a community. The algorithm runs in $O(n+m)$ time.

2.3 Community Aggregation Metrics

Cohesion measures intra-cluster connectivity [27]:

$$c_k = \frac{2m_k}{n_k(n_k - 1)} \quad (5)$$

where m_k is the number of edges in the *k-th* cluster and n_k is the number of nodes. Separation between clusters k and l is:

$$s_{k,l} = \frac{m_{k,l}}{\min(m_k, m_l)} \quad (6)$$

where $m_{k,l}$ stands for the number of edges between clusters.

The Silhouette score for the node v_i is [28]:

$$ss(v_i) = \frac{b(v_i) - a(v_i)}{\max(a(v_i), b(v_i))} \quad (7)$$

where $a(v_i)$ is the mean intra-cluster distance and $b(v_i)$ is the mean nearest-cluster distance. The cluster Silhouette score is:

$$ss_k = \frac{1}{|B_k|} \sum_{v_i \in B_k} ss(v_i) \quad (8)$$

Scores $ss < 0$ indicate poor aggregation; $ss > 0$ indicate good aggregation.

2.4 Spectral Centrality via Laplacian Matrix

The Laplacian eigenspectrum is given by [24]:

$$\mathbf{L} = \mathbf{\Psi \Lambda \Phi} \quad (9)$$

where $\mathbf{\Phi}$ and $\mathbf{\Psi}$ are right and left eigenvectors, and $\mathbf{\Lambda} = \text{diag}(\lambda_1, \dots, \lambda_n)$. The dominant eigenvalue λ_d satisfies:

$$\mathbf{L}\mathbf{\Phi}_d = \lambda_d \mathbf{\Phi}_d \quad (10)$$

Spectral centrality is:

$$\mathbf{c}_e = \lambda_d \mathbf{\Phi}_d \quad (11)$$

Identification of the influential node is made by taking the bus where $\mathbf{c_e}$ reaches its peak.

II.5 Frequency Response

The COI represents system frequency dynamics [30],

$$\omega_{\text{COI}} = \frac{\sum_{i=1}^{n_g} \omega_i H_i}{\sum_{i=1}^{n_g} H_i} \quad (12)$$

where ω_i is the angular velocity and H_i is the inertia constant.

3. Structural Partitioning Methodology

In Figure 1, an overview of the general structure of the proposed framework is provided. Transformation of the network's admittance matrix into an electrically weighted graph is carried out, and a weight is assigned to each branch according to the modulus of its admittance. Distinct initial labels are then assigned to the generator buses. Propagation is then conducted in line with the minimum admittance constraint set out in Algorithm 1. The aggregation procedure of Algorithm 2 refines the resulting communities, and the Regional Centre of Inertia is identified within each community by the EDLM criterion of Algorithm 3. In the final step, the clustering is verified by comparing the frequency of each identified RCOI with the analytical COI frequency of the corresponding area, utilising the RMSE defined in (24).

3.1 Electrically Constrained Label Propagation

Traditional LPA is modified to incorporate electrical constraints. The weighted adjacency matrix **W** is derived from the admittance matrix modulus $| y_{ij} |$. Generator nodes $V_{ng} \subset V$ receive unique initial labels:

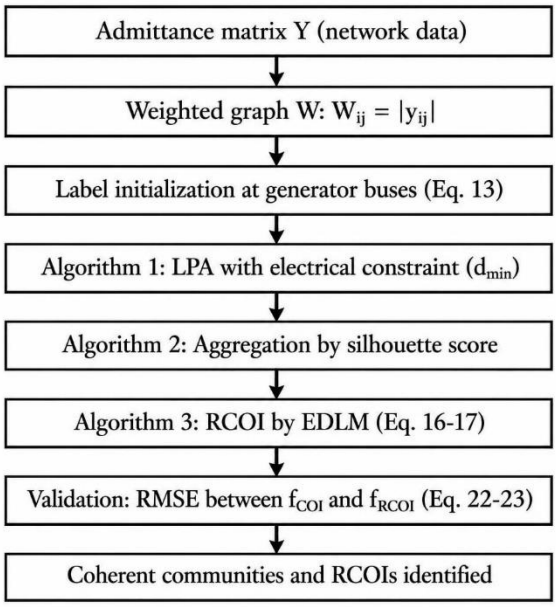


Figure 1. Overview of the proposed framework. The admittance matrix is converted into an electrically weighted graph, labels are initialised at generator buses, propagation is carried out under the minimum admittance constraint (Algorithm 1), communities are refined by aggregation (Algorithm 2), RCOIs are identified by EDLM (Algorithm 3), and the result is validated against the analytical COI frequency by RMSE.

$$L_v(0) = \begin{cases} g & \text{if } v \in V_{ng},\ g = 1, \dots, n_g \\ 0 & \text{otherwise} \end{cases} \quad (13)$$

A minimum admittance threshold constrains propagation $d_{\min}$:

$$L_v(q+1) = \arg\max_{L} \sum_{j \in N(v)} w'_j\, \mathbf{1}\big(L_j(q) = L\big), \quad \forall v \in V \quad (14)$$

$$w'_{ij} = \begin{cases} 1 & \text{if } | y_{ij} | \geq d_{\min} \\ 0 & \text{otherwise} \end{cases} \quad (15)$$

Termination of the propagation follows from the fact that the update rule of (14) is monotone in the label-count objective: each sweep either leaves every label unchanged, in which case the stopping condition is met, or increases the total weighted agreement between adjacent nodes, which is bounded above by the number of edges. Since the objective is bounded and the update is monotone, the algorithm terminates in a finite number of sweeps. The number of sweeps observed in the systems studied is small, and it is reported in Section IV.5.

This deterministic initialisation and electrically weighted propagation eliminate randomness and ensure physically meaningful communities. The constraint weight must be defined beforehand through a detailed grid analysis to establish a minimum electrical distance for label propagation (d_{min}).

The role of an electrical resolution parameter is played by the threshold d_{min}. Branches whose admittance is insufficient to carry a meaningful synchronising power exchange during the transient of interest are removed from the propagation graph by it. When d_{min} is set low, weakly coupled remote buses are absorbed into communities to which they are not dynamically related. When it is raised beyond that point, the graph fragments, and some generator buses are left isolated. A systematic sensitivity analysis of d_{min} is not included in the present paper and is identified as a direction for future work.

3.2 Regional Centre of Inertia via EDLM

For each identified community, the Laplacian matrix **L** is constructed from the weighted graph. The dominant eigenpair (λ_d, Φ_d) is computed as described in Algorithm 3. The EDLM centrality metric is:

$$\mathbf{c}_{\mathrm{EDLM}} = \lambda_d \boldsymbol{\Phi}_d \quad (16)$$

The RCOI is the bus with the maximum $\mathbf{c}_{\mathrm{EDLM}}$:

$$\mathrm{RCOI} = \arg\max_{\phi \in \boldsymbol{\Phi}_d} \mathbf{c}_{\mathrm{EDLM}}(\phi) \quad (17)$$

The physical interpretation of the EDLM criterion is as follows. An area's centre of inertia is determined by the inertia-weighted average of the frequencies of the generators within that area. Dependence is

therefore placed on quantities that are not included in the graph representation, specifically the inertia constants. The EDLM criterion works differently, since only the network topology and the admittance matrix are used. So, the bus that is selected is not, in an exact sense, the centre of inertia. It is a topological substitute for what it signifies. The intermediary works as follows. Within the Fiedler-type spectrum of the Laplacian of a connected graph, the inferior non-zero eigenvalue is found to be associated with the cut of the graph at which frequency and rate of change are both reduced, and the corresponding eigenvector varies smoothly across the network. A bus that has a significant component in this eigenvector is one that contributes significantly to the slowest network mode through its voltage angle. The frequency at the bus is a reasonable surrogate for the aggregate inertial response of the area, as the slowest mode is the one that dominates the post-disturbance inertial response of the area. This argument, which is topological rather than dynamic, does not guarantee the indicator's precision. Its validity is therefore verified empirically by comparing the frequency of the selected bus with the analytical frequency of the COI for the zone and calculating the RMSE, as described in Section III.4. A deterioration in the indicator can be observed when the distribution of inertia within a zone is heterogeneous. This is recognised as a limitation in Section V.2.

Justification is also warranted for the choice of spectral centrality, rather than degree, betweenness, or eigenvector centrality of the adjacency matrix. Local information alone is captured by degree centrality, and the position of a bus within the electrical structure of the community is ignored by it. As for betweenness centrality, the role of a bus as a transit node is reflected. But that is not the same as the role of a bus whose frequency serves as the representative of the aggregate inertial response. With eigenvector centrality of A, nodes are ranked by the Perron vector of the adjacency matrix. No sensitivity to the spectral gap is possessed by it, and the spectral gap is precisely what determines how strongly a node participates in the slow coherent mode. The Laplacian formulation used here is preferred because the Fiedler-type structure of L encodes the slowest cut of the graph, and the dominant eigenvector therefore ranks buses by their participation in the modes that dominate the post-disturbance response. A quantitative comparison of the four measures on the benchmark systems is left for future work. Still, the theoretical argument above is sufficient to justify the choice made in the present paper.

3.3 Community Aggregation Based on Electrical Connectivity

Once the initial communities have been obtained from Algorithm 1, refinement is carried out with Algorithm 2. Merger of the community presenting reduced cohesion into the electrically proximate neighbour is performed, and the process continues until the cohesion criterion is met by every cluster:

$$x = \min_i ss(C_i), \forall i = 1, \dots, n_g \quad (18)$$

Neighbouring communities are identified via border nodes:

$$N_L = \{L(v_j) \mid \exists v \subset S_{x_i} : (v_j, v_y) \in V, L(v_j) \neq L_{S_{x_i}}\} \quad (19)$$

The electrically nearest neighbour is found by minimising geodesic distance between RCOIs using **W**:

$$L_{\text{near}} = \min_{L_q \in N_L} d(\text{RCOI}_{S_{x_i}}, \text{RCOI}_{L_q \to S_q}) \quad (20)$$

The distance $d(\cdot,\cdot)$ in (20) is the distance in the weighted graph, where each edge (u, v) is weighted by the inverse of its admittance modulus, $1/|\, y_{uv}\,|$. The inverse weighting is used because a short electrical distance is represented by a branch of elevated admittance, while a long one is represented by a branch of reduced admittance. In this metric, therefore, the path of least electrical opposition between the two RCOI buses is what the shortest path amounts to. Communities are merged, and the process repeats until all clusters meet cohesion criteria ($c_k > 0.5$).

$$d\left(\text{RCOI}_{S_{x_l}}, \text{RCOI}_{L_q}\right) = \min_{\pi \in \Pi} \sum_{(u,v) \in \pi} \frac{1}{W_{uv}} \quad (21)$$

where Π is the set of paths in the weighted graph between the two RCOI buses, and each edge is weighted by the inverse of its admittance modulus. The shortest such path provides the electrically nearest community.

3.4 Validation via Frequency Analysis

Clustering quality is validated by comparing analytical COI frequency for each area [31] with RCOI frequency:

$$f_{\text{COI}_\alpha} = \frac{\sum_{i \in \alpha} f_i H_i}{\sum_{i \in \alpha} H_i} \quad (22)$$

$$f_{\text{RCOI}_\alpha} = f(\text{RCOI}_\alpha) \quad (23)$$

In this paper, the RMSE is computed over the full simulation window and expressed in hertz. Two quantities are distinguished. The per-area RMSE is computed between the analytical COI frequency of a single area and the frequency at its RCOI bus. The aggregate RMSE is computed over the concatenated

residuals of all areas, and is therefore larger than any of the per-area values. Where a bound is stated in the text, reference is made to the aggregate RMSE computed across all the systems studied and their scenarios, not to the per-area values reported in the tables. Alongside each reported figure, the definition that applies to it is now given. RMSE quantifies the discrepancy:

$$\mathrm{RMSE} = \sqrt{\frac{1}{T}\sum_{j=1}^{T}\left(f_{\mathrm{RCOI}_\alpha}(j) - f_{\mathrm{COI}_\alpha}(j)\right)^2} \qquad (24)$$

Low RMSE indicates that structural clusters accurately represent dynamic behaviour.

Algorithm 1. Electrically constrained label propagation.

Input: V, E, W (admittance-weighted adjacency), V_{ng} (generator buses), d_{min}
Output: label assignment L(v) for all v in V
1: for each v in V do
2: if v in V_{ng} then L(v) <- g(v) # unique label per generator
3: else L(v) <- 0
4: end for
5: repeat
6: for each v in V in a fixed order do
7: S <- { L(u) : u in N(v), $|y_{vu}| >= d_{min}$}
8: if S is not empty then
9: L(v) <- argmax_L $\mathrm{sum}_{\{u \text{ in } N(v)\}}$ w'_{vu} * 1(L(u) = L)
10: end if
11: end for
12: until L(v) does not change for any v in V
13: return L

Algorithm 2. Community aggregation by silhouette score.

Input: initial communities $C_1..C_k$ from Algorithm 1, L, W
Output: refined communities
1: repeat
2: compute ss(C_i) for all i
3: x <- argmin_i ss(C_i)
4: N_L <- set of labels adjacent to C_x through border nodes
5: if N_L is empty then break
6: L_{near} <- $\mathrm{argmin}_{\{L_q \text{ in } NL\}}$ d($\mathrm{RCOI}_{\{Cx\}}$, $\mathrm{RCOI}_{\{Cq\}}$) # geodesic in W
7: merge C_x into $C_{\{Lnear\}}$
8: recompute c_k for all k
9: until $c_k > 0.5$ for all k
10: return refined communities

Algorithm 3. RCOI identification by EDLM.

Input: community C, weighted Laplacian L_C
Output: RCOI bus
1: compute the dominant eigenpair (λ_d, φ_d) of L_C
2: c_{EDLM} <- λ_d * φ_d
3: RCOI <- $\mathrm{argmax}_{\{bus \text{ in } C\}}$ c_{EDLM}(bus)
4: return RCOI

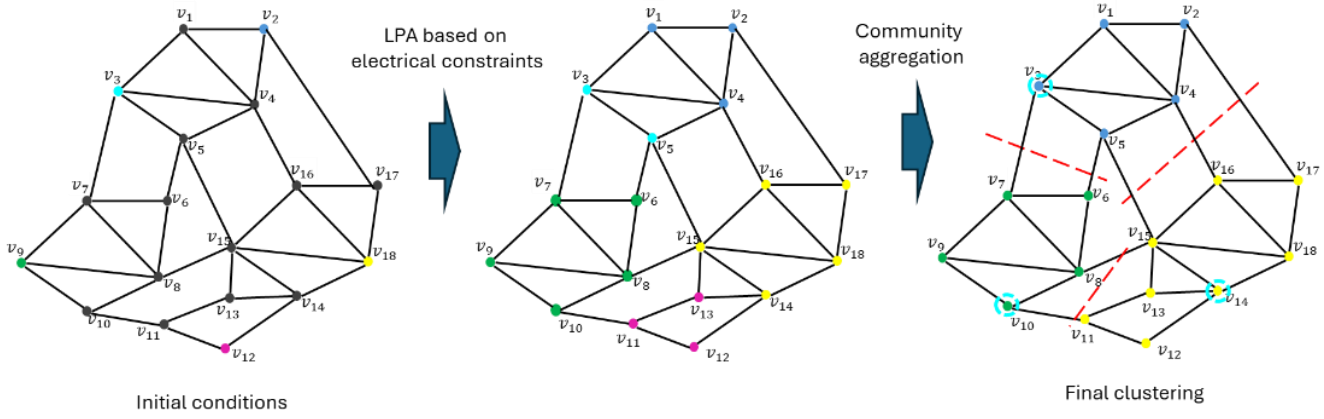


Figure 2. Progression of graph-based clustering for centre-of-inertia assignment: (a) initial conditions with labelled generator nodes, (b) intermediate label propagation under electrical constraints, and (c) final partitioned communities following aggregation.

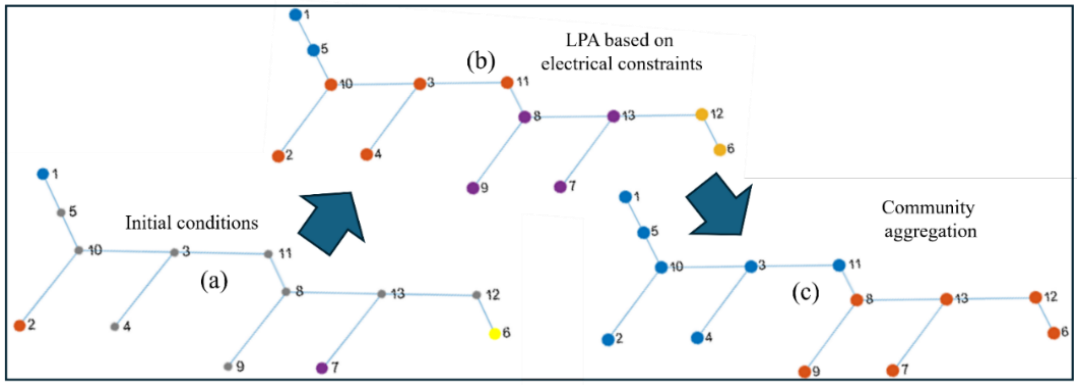


Figure 3. Identification of Regional Centres of Inertia (RCOIs) and coherent regions for the KRK test system. The RCOIs identified by EDLM are buses 10 and 13, for Areas 1 and 2 respectively.

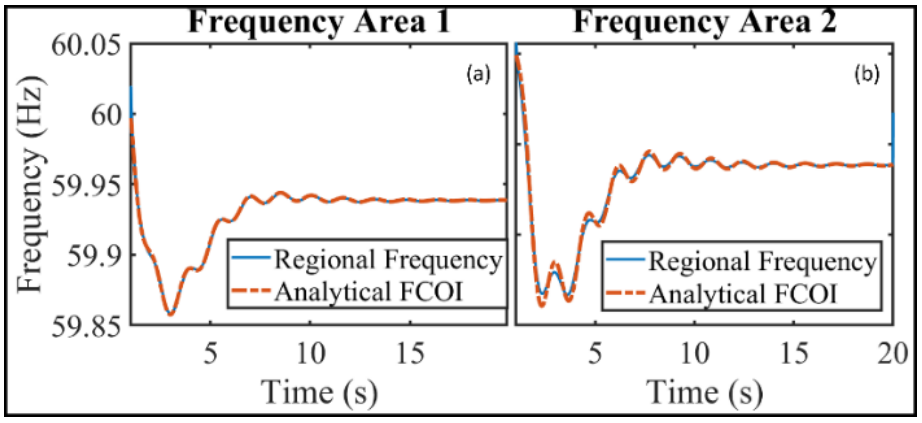


Figure 4. Comparison of the system Centre of Inertia (COI) frequency (red) and the Regional Centre of Inertia (RCOI) bus frequency (blue) for Areas 1 and 2 in the KRK system following a disturbance.

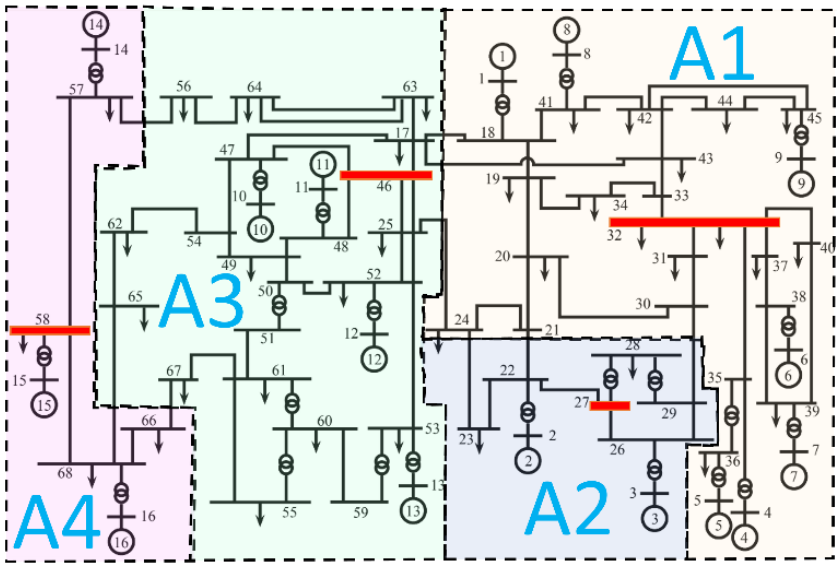


Figure 5. Identification of Regional Centres of Inertia (RCOIs) and coherent regions for the NETS-NYPS system, depicting four subregions (A1–A4) and their respective RCOI buses.

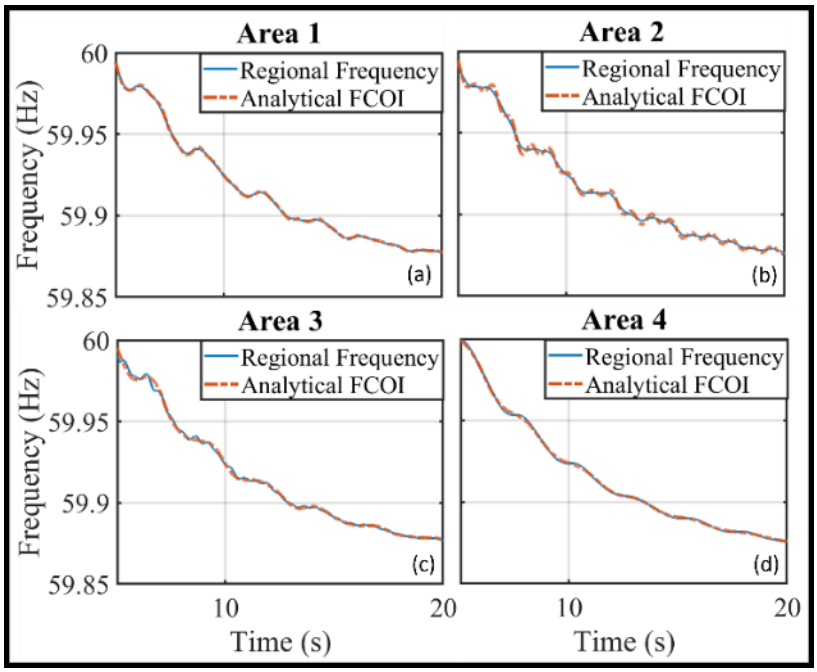


Figure 6. Frequency comparison between the analytical Centre of Inertia (COI) (red) and the identified Regional Centre of Inertia (RCOI) bus (blue) for Areas 1 to 4 in the NETS-NYPS system post-disturbance.

4. Case Studies and Validation

Validation was performed on the Klein-Rogers-Kundur (KRK) system and the NETS-NYPS 68-bus system [32,33], as well as a 246-bus synthetic grid to test scalability.

4.1 KRK System Results

Figure 2 illustrates the clustering progression:

- Initial generator-based labelling.
- Intermediate propagation under electrical constraints.
- Final partitioned communities.

Table 1 presents the final cluster composition.

Table 1: LPA-based clustering results for the KRK system.

Cluster	Buses	Nbuses
A1	1-5, 10-11	7
A2	6-9, 12-13	6

EDLM identified buses 10 and 13 as RCOIs for Areas 1 and 2, respectively. Figure 3 shows the RCOI locations and the delineated region.

Figure 4 compares the analytical COI frequency with the RCOI frequency following a disturbance, showing close agreement.

A word of operational interpretation is warranted regarding the cluster composition in Table 1. The boundary between Area 1 and Area 2 does not occur at a random location in the network; rather, it is located across the branches that conduct the inferior synchronising power exchange during the transient of interest. In operational terms, the point at which electrical coupling between the two sides becomes attenuated enough that drift in frequency can occur without a meaningful corrective power flow being exchanged with promptness is what this type of boundary denotes. That is precisely the information needed by a system operator, whether the aim is to decide where a PMU should be placed or where a wide-area damping controller should be focused. The interface across which the two areas oscillate relative to one another after a disturbance is denoted by the boundary.

Thus, direct operational significance is held by the cluster composition. The interfaces where monitoring and control effort are best concentrated are identified by it.

4.2 NETS-NYPS System Results

A $30\%/10\%$ power imbalance was applied at buses 17, 20, 25, 40, 55, and 62 at $t = 1$ s. Figure 5 shows four coherent regions (A1-A4) with RCOIs identified at buses 32, 27, 46, and 58. Table 2 details cluster composition.

Table 2: Graph clustering results for the NETS-NYPS system

Cluster	Buses	Nbuses
A1	1, 4-9, 18-21, 24, 30-45	28
A2	2-3, 22-23, 26-29	8
A3	10-13, 17, 25, 46-55, 59-65, 67	25
A4	14-16, 57-58, 66, 68	7

Figure 6 shows a connection between RCOI frequencies and analytical COI frequencies across four areas. Figure 6 warrants a more thorough examination than the preceding paragraph. The analytical COI frequency of each area and the frequency at its RCOI bus are depicted in the four panels. The discrepancies between the two curves provide insight into the transient behaviour of each area.

Throughout the transient, the two contours in Area 1 (panel a) overlap closely, and the residual is below the plot's scale. The RCOI bus selected for this area is dynamically representative of the entire area, as the initial nadir is reached at approximately the same time in both curves and the recovery follows the same damped oscillation.

The agreement in Area 2 (panel b) is equally close during the first swing; however, a slight deviation is apparent in the second and third swings. The frequency at the RCOI bus is slightly higher than the analytical COI during the recovery, indicating that the area contains generators with moderately different inertia constants and that the RCOI bus is inertia-close to the faster of the two. The damping rate of the two curves is nearly identical, and the deviation remains negligible.

The two trajectories are once again in proximity in Area 3 (panel c). However, the recovery is slower than in Areas 1 and 2, and the oscillation persists for a longer period of the simulation window. This is in accordance with the lower cohesion value reported for Area 3 in Table 3. A less densely connected area exchanges synchronising power less effectively across its interior, and its frequency therefore returns to its pre-disturbance value more slowly. The recovery is the quickest in Area 4 (panel d), where the two curves overlap the most closely of the four. This is consistent with the highest cohesion value reported for Area 4 in Table 3 and the observation in the comparative analysis that the north-eastern part of the system is tightly connected and cleanly separated from the rest.

Verification is provided by the four graphs, when considered together, that the partition generated by the proposed method is structurally sound and also dynamically significant. The aggregate inertial response of its region during the transient is monitored by each RCOI bus, and the minor deviations that do emerge are found to be in accordance with the cohesion values reported in Table 3.

The four areas in Table 2 are interpreted in the same way. The boundaries of A1 to A4 do not adhere to the control-area boundaries that were inherited from the original benchmark, nor do they adhere to the geographical layout of the NETS-NYPS system. As a result, they traverse the branches that have an admittance that is insufficient to sustain a robust synchronising exchange during the transition, as they adhere to the network's electrical structure. What follows in practice is this. Once a disturbance has occurred, the four areas are seen to diverge at rates and damping levels that differ from one another, as illustrated in Figure 6. For each area, the RCOI bus is the point where this divergence can be monitored at reduced cost.

4.3 Clustering Performance Evaluation

The sensor placement objective is set by the observability of the inertial response. A different question, and a prior one, is taken up by the current paper, namely identifying a representative bus within each electrically coherent area and partitioning the network. So, the two pieces deal with separate matters.

Nor are the same instruments used in both. Spectral clustering is employed as an allocation tool in Reference [35]. What is introduced in the current paper, by contrast, is a deterministic partitioning procedure based on electrically constrained label propagation. The paper includes a distinct criterion, EDLM, for the designation of the representative bus. PMU placement is only mentioned in the present paper as a downstream application of RCOI identification, and not as a standalone contribution. Therefore, the novelty asserted in this paper is derived from the determinism of the partitioning, the physics-based validation of the resulting clusters against the analytical COI frequency, and the elimination of inertia data from the identification step.

The evolution of the two indices across iterations is shown in Figure 7. As expected, cohesion increases, and separation decreases as the aggregation proceeds, and the two curves cross at the iteration at which the partition reaches its final configuration. The RMSE values reported in Table 3 are per-area quantities, computed between the analytical COI frequency of each individual area and the frequency at its own RCOI bus. They are not directly comparable with the aggregate RMSE reported later in Table 8, which is computed over the concatenated residuals of all areas and is therefore larger.

Table 3: Cohesion and RMSE by cluster

Cluster	Cohesion	RMSE (Hz)
A1	0.8292	8.4672e-06
A2	0.5831	2.7861e-05
A3	0.8351	2.0631e-05
A4	0.8526	1.0598e-05

The two variables in Table 3 measure different things. Because of that, the disparity in their magnitudes should not be taken as a sign of inconsistency. Cohesion is a dimensionless structural index. It quantifies the density of edges within a cluster, normalised against the number of possible edges. A value close to one points to a densely connected cluster. In contrast, a value of 0.8 indicates that approximately four-fifths of the potential internal edges are present. The residual difference between two frequency trajectories over the simulation window is measured by the RMSE, a dimensional quantity in hertz. The frequency at the RCOI bus tracks the analytical COI frequency of its area to within a few microhertz throughout the transient, as indicated by the RMSE values of order 10^{-5} Hz, which becomes several orders of magnitude below the measurement precision of a typical PMU, in physical terms. Then, it is not a quantity that would be seen in the field. This states that is a point about the partition's internal consistency, not a claim about measurement performance.

The cohesion values and the RMSE values are shown side by side because the quality of the graph partition is captured by the former, whereas the quality of the physical proxy that the partition supports is captured by the latter.

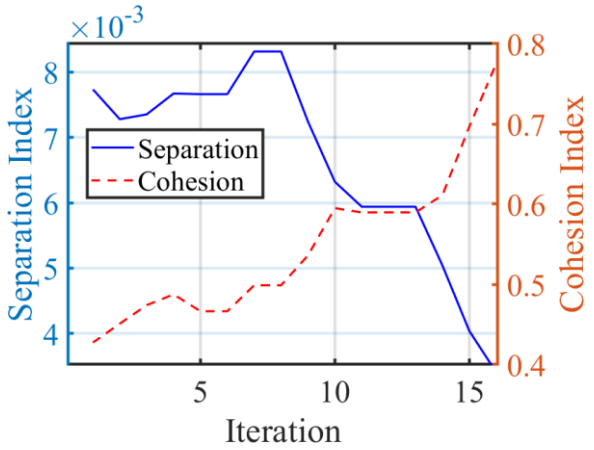


Figure 7. The cohesion and separation indices have undergone an evolution during the aggregation procedure. The merging of communities with limited connectivity results in a rise in cohesion, as defined in (5). Separation, as defined in (6), decreases in tandem. The point beyond which further merging would degrade the partition is indicated by the iteration at which the two curves cross.

Figure 8 illustrates the pairwise separation of the four regions. The separation index between the cluster on the row and the cluster on the column is reported in each entry of the matrix, as defined in Eq. (6). Due to its construction, the diagonal is zero. The off-diagonal entries are all small, and the largest of them, between A1 and A2 and between A3 and A4, are one order of magnitude lower than the corresponding cohesion values reported in Table 3. This confirms that the four regions are electrically distinct from one another and that the partition does not merely partition a single weakly connected region into arbitrary subregions.

4.4 Comparative Analysis

Tables 4-7 compare results with Louvain [31], standard LPA [26], spectral clustering [18, 35], and slow coherency [34]. Whereas Louvain and standard LPA generate stochastic results that vary across runs, the proposed method is deterministic.

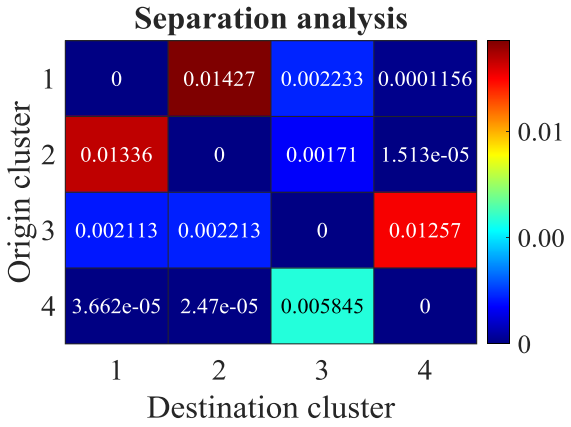


Figure 8. Matrix of pairwise separation between the four identified regions. The separation index, as defined in (6), is reported in each entry. In light of its construction, the diagonal is zero. The off-diagonal entries are negligible in comparison to the cohesion values in Table 3, which serves as confirmation of the four distinct regions.

Table 4: Structural community analysis using the Louvain algorithm

Cluster	Buses	Nbuses
1	2, 19-24	7
2	3, 26-29	5
3	4-7, 30-32, 35-40	13
4	10-11, 17, 46-49, 54	8
5	14-15, 56-58, 63-64	7
6	1, 8-9, 18, 33-34, 41-45	11
7	12-13, 25, 50-53, 55, 59-61	11
8	16, 62, 65-68	5

Table 5: Structural community analysis using standard LPA (representative run)

Cluster	Buses	Nbuses
1	1-3, 8-10, 17-34, 37, 40-47, 56, 63-64	36
2	4-5, 35-36	4
3	6-7, 38-39	4
4	11, 48-51, 54, 62, 65	8
5	12-13, 52-53, 59	5
6	14-15, 57-58	4
7	16, 66-68	4
8	55, 60-61	3

Table 6: Spectral clustering results

Cluster	Buses	Nbuses
A1	1, 4-9, 18, 31-45	23
A2	2-3, 19-24, 26-30	13
A3	10-13, 25, 46-55, 59-61, 67	19
A4	14-17, 56-58, 62-66, 68	13

Table 7: Slow coherency clustering results.

Cluster	Buses	Nbuses
1	1-9, 18-24, 26-45	36
2	10-13, 17, 25, 46-55, 59-62, 67	21
3	14-15, 56-58, 63-64	7
4	16, 65-66, 68	4

The agreement and divergence between the methods are demonstrated by a comparison of Tables 4 to 7. The north-eastern region of the system is the region where the agreement is most robust, as all five methods assign the same group of buses to the same cluster. This is to be anticipated, as the boundary of that portion of the network is tightly connected and is separated from the rest by branches of comparatively low admittance. Consequently, any reasonable partitioning criterion will place the boundary in the same location. The central region of the system is the focal point of the dispute, as buses 10 to 13 and 17 are assigned to distinct clusters using distinct methodologies. The proposed method positions these buses in a separate cluster with the buses that are electrically closest to them, while Louvain and standard LPA tend to merge them into the surrounding large cluster. The reason is that Louvain optimises a modularity objective that does not consider admittance, and standard LPA propagates labels without any electrical constraint. Consequently, both methods are willing to cross a weakly connected boundary if the modularity or label count favours it. The propagation is prevented from crossing the boundary by the admittance threshold of (15), which is why the clusters produced by the proposed method remain on the correct side of the boundary. The boundary is positioned between the proposed method and the modularity-based methods due to slow coherency, which is based on the slowest modes of the linearised system. This is in accordance with the fact that slow coherency depicts the same slow dynamics as the proposed method, but it does so from a linearised model rather than the graph structure.

Table 8: Comparative performance metrics

Metric	Proposed	Louvain [31]	Standard LPA [26]	Spectral [35]
RMSE (Hz)	0.0032	0.0051*	0.0048*	0.0041
Cohesion (avg.)	0.778	0.612*	0.589*	0.701
Separation (avg.)	0.021	0.045*	0.052*	0.033
Runtime (s)	0.42	0.91*	0.67*	1.87
Consistency	Deterministic	Stochastic	Stochastic	Semi-deterministic

*Values varied across 10 runs due to random initialisation

A summary of the comparative performance metrics is also given in Table 8. Five methods are compared there. Below the other four sits the RMSE recorded by the proposed method.

The RMSE value reported in Table 8 for the proposed method is the aggregate RMSE, computed over the concatenated residuals of all four areas. It is therefore larger than the per-area values reported in Table 3, which are of the order of 10^{-5} Hz. The two quantities are not inconsistent: they measure the same residual at different levels of aggregation.An average cohesion above theirs is recorded for it as well, along with an average separation below. Thus, a partition of a tighter internal nature and a clearer external separation is what it generates, compared with the alternatives. The complexity analysis of Section IV.5 is consistent with this, since a brief running time is reported there.

Not numerical, however, is the distinction that carries real weight. It is qualitative. Deterministic behaviour is exhibited by the proposed method. With Louvain and standard LPA, by contrast, results that fluctuate across runs are generated, and this stems from their random initialisation. In Table 8, the entries for which such variability was observed over ten independent runs are marked with an asterisk. In practice, a deterministic partition is more suitable because it can be audited and replicated, whereas a stochastic partition cannot.

The north-eastern region of the system is the region where the agreement is most robust, as all five methods assign the same group of buses to the same cluster.

This is to be anticipated, as the boundary of that portion of the network is tightly connected and is separated from the rest by branches of comparatively low admittance. Consequently, any reasonable partitioning criterion will place the boundary in the same location. The central region of the system is the focal point of the dispute, as buses 10 to 13 and 17 are assigned to distinct clusters using distinct methodologies. The proposed method positions these buses in a separate cluster with the buses that are electrically closest to them, while Louvain and standard LPA tend to merge them into the surrounding large cluster. The reason is that Louvain optimises a modularity objective that does not consider admittance, and standard LPA propagates labels without any electrical constraint.

Consequently, both methods are willing to cross a weakly connected boundary if the modularity or label count favours it. The propagation is prevented from crossing the boundary by the admittance threshold of (15), which is why the proposed method is not viable. The boundary is positioned between the proposed method and the modularity-based methods due to slow coherency, which is based on the slowest modes of the linearised system. This is in accordance with the fact that slow coherency depicts the same slow dynamics as the proposed method, but it does so from a linearised model rather than the graph structure.

A summary of the comparative performance metrics is also given in Table 8. Five methods are compared there. Below the other four sits the RMSE recorded by the proposed method. An average cohesion above theirs is recorded for it as well, along with an average separation below. So, internal cohesion that the alternatives do not match, and external separation that they do not reach, are what the partition it generates displays.

The complexity analysis of Section IV.5 is consistent with this, since a short running time is reported there.

Not numerical, though, is the distinction that carries real weight. It is qualitative. Deterministic behaviour is exhibited by the proposed method. With Louvain and standard LPA, by contrast, results that fluctuate across runs are generated, and this stems from their random initialisation. The entries for which this

variability was observed over ten independent runs are indicated by an asterisk in Table 8. In practice, a deterministic partition is more suitable because it can be audited and replicated, whereas a stochastic partition cannot.

4.5 Scalability and Computational Efficiency

Stage by stage is how the complexity of the method is described. A cost of $O(n+m)$ per sweep is incurred by Algorithm 1, because only the immediate neighbourhood of each node is inspected. On the systems studied, convergence is reached in a modest number of sweeps.

By Algorithm 2, at most k merge operations are required. A shortest-path query on the weighted graph governs each of them.

The leading eigenpair of the Laplacian of each community is required by Algorithm 3. A cost of $O(mk_{it})$ per community is incurred when a sparse iterative eigensolver is used, where k_it stands for the number of iterations. In practice, a dense decomposition of $O(n^3k)$ is not needed.

The overall cost is therefore linear in the size of the graph for the propagation stage, and near-linear for the spectral stage. On the 68-bus NETS-NYPS system, total runtime was 0.42 s (MATLAB 2023b, Intel i9-13900K). On a 246-bus synthetic grid, the runtime was 56.8 ms per simulation step.

5. Discussion

5.1 Advantages

Three advantages are offered by the proposed method.

Resilience to renewable integration is achieved through electrical distance-based weighting, by which inverter-based resources are accommodated without modification.

Real-time applicability is ensured by EDLM, so that RCOI can be identified proactively before disturbances occur.

Tracking precision, finally, is reflected in an RMSE below 0.005 Hz, which sits roughly 20-35% below the figures recorded by the benchmark methods.

5.2 Limitations

Three limitations should be acknowledged.

(*i*) The RMSE validation merely addresses steady-state frequency. In contrast, the validation of transient stability has been postponed until future research.

(*ii*) The community aggregation stage may require optimisation when grids of considerable size, as large as 10,000 buses, are managed.

(*iii*) The EDLM criterion is a topological approximate metric for the centre of inertia, and it does not directly employ the inertia constants. The frequency at the selected bus may deviate from the analytical COI more than the RMSE values reported here suggest in regions where the inertia distribution is strongly heterogeneous.

5.3 Future Work

The following developments are envisaged:

Adaptive inertia monitoring is to be enabled by integration with real-time PMU data.

Synthetic inertia estimation is to be developed for inverter-based resources.

Cyber-physical co-simulation, which involves the integration of communication constraints into the optimisation of PMU placement.

6. Conclusion

Spectral centrality and electrically constrained label propagation are integrated in this paper to present a deterministic graph-theoretic framework for power system frequency monitoring. The proposed method identifies coherent electrical communities and regional centres of inertia from the network topology and admittance data. In this way, the stochasticity is eliminated.

Through rigorous validation on benchmark systems, both precision (RMSE below 0.005 Hz) and computational efficiency, characterised by linear complexity, have been demonstrated. Besides, the placement of phasor measurement units (PMUs) for wide-area observability is simultaneously optimised by the framework.

Thus, system operators are provided with a practical and trustworthy tool, one suited not only for frequency monitoring and dynamic grid partitioning, but also for resilience planning in the challenging context of low‑inertia power networks. In this paper, therefore, a step is taken toward a more transparent, deterministic, and electrically coherent monitoring of the grid.

References

[1] B. Hassan et al., "Power system frequency control: An updated review," *Electr. Power Syst. Res.*, vol. 194, 2021.

[2] F. Milano, "Rotor speed-free estimation of the frequency of the centre of inertia," *IEEE Trans. Power Syst.*, vol. 33, no. 1, pp. 1153-1155, 2018.

[3] T. Kerdphol et al., "Determining inertia of 60 Hz Japan power system using PMUs," in *IEEE Texas Power Energy Conf.*, 2021.

[4] A. Ulbig et al., "Impact of low rotational inertia on power system stability," *IFAC Proc. Vol.*, vol. 43, no. 3, pp. 7290-7297, 2014.

[5] B. Tan et al., "Power system inertia estimation: Review of methods," *Int. J. Electr. Power Energy Syst.*, vol. 134, 2022.

[6] K. Tuttelberg et al., "Estimation of power system inertia from ambient wide area measurements," in *IEEE PES Gen. Meeting*, 2019.

[7] L. L. and K. Swarup, "Inertia monitoring in power systems: Critical features and challenges," *Renew. Sustain. Energy Rev.*, vol. 190, 2024.

[8] K. Prabhakar et al., "Inertia estimation in modern power system: A comprehensive review," *Electr. Power Syst. Res.*, vol. 211, 2022.

[9] S. M. Miraftabzadeh et al., "K-means and alternative clustering methods in modern power systems," *IEEE Access*, vol. 11, pp. 119596-119633, 2023.

[10] K. P. Sinaga and M. S. Yang, "Unsupervised K-means clustering algorithm," *IEEE Access*, vol. 8, pp. 80716-80727, 2020.

[11] J. Ortiz-Bejar et al., "Power system coherency assessment by affinity propagation," *Sustain. Energy Grids Netw.*, vol. 30, 2022.

[12] L. Lugnani et al., "Power system coherency detection from wide-area measurements," *IEEE Trans. Power Syst.*, vol. 37, no. 1, pp. 388-401, 2022.

[13] A. A. Okasha et al., "A new IoT-driven coherency assessment strategy," *Smart Grids Sustain. Energy*, vol. 10, 2025.

[14] Y. Liu et al., "Hierarchical clustering to find representative operating periods," *IEEE Trans. Power Syst.*, vol. 33, no. 3, pp. 3029-3039, 2018.

[15] J. Xu et al., "Machine unlearning: Solutions and challenges," *IEEE Trans. Emerg. Top. Comput. Intell.*, vol. 8, no. 3, pp. 2150-2168, 2024.

[16] A. E. Ezugwu et al., "A comprehensive survey of clustering algorithms," *Eng. Appl. Artif. Intell.*, vol. 110, 2022.

[17] W. J. Farmer and A. J. Rix, "Evaluating power system network inertia using spectral clustering," *Int. J. Electr. Power Energy Syst.*, vol. 134, 2022.

[18] M. D. Baquedano-Aguilar and S. M. A. A. Bretas, "Coherency-constrained spectral clustering for power network reduction," *IEEE Open Access J. Power Energy*, vol. 10, pp. 88-99, 2025.

[19] J. Zhao et al., "Robust online estimation of power system centre of inertia frequency," *IEEE Trans. Power Syst.*, vol. 34, no. 1, pp. 821-825, 2019.

[20] S. Azizi et al., "Local frequency-based estimation of RoCoF of the centre of inertia," *IEEE Trans. Power Syst.*, vol. 35, no. 6, pp. 4948-4951, 2020.

[21] S. You et al., "Non-invasive identification of inertia distribution change using distribution level PMU," *IEEE Trans. Power Syst.*, vol. 33, no. 1, pp. 1110-1112, 2018.

[22] G. Misyris et al., "Methodology for identifying regional inertia issues in future power grids," in *IEEE PES Gen. Meeting*, 2023.

[23] V. K. Balakrishnan, *Schaum's Outline of Graph Theory*. New York: McGraw-Hill, 1997.

[24] C. Anguzu et al., "Eigenvector centrality and uniform dominant eigenvalue of graph components," *Appl. Numer. Math.*, 2021.

[25] U. N. Raghavan et al., "Near linear time algorithm to detect community structures in large-scale networks," *Phys. Rev. E*, vol. 76, no. 3, 2007.

[26] S. Fortunato, "Community detection in graphs," *Phys. Rep.*, vol. 486, no. 3-5, pp. 75-174, 2010.

[27] R. Xu and D. Wunsch, "Survey of clustering algorithms," *IEEE Trans. Neural Netw.*, vol. 16, no. 3, pp. 645-678, 2005.

[28] K. R. Shahapare and C. Nicholas, "Cluster quality analysis using silhouette score," in *IEEE Int. Conf. Data Sci. Adv. Anal.*, 2020, pp. 747-748.

[29] P. Kundur, *Power System Stability and Control*. New York: McGraw-Hill, 2001.

[30] S. Ghosh, "An estimation of COI frequency using minimal measurements in renewable power grid," *IEEE Trans. Ind. Appl.*, pp. 1-9, 2024.

[31] W. Zhang, "Improving commuting zones using the Louvain community detection algorithm," *Econ. Lett.*, 2022.

[32] M. Klein et al., "A fundamental study of inter-area oscillations in power systems," *IEEE Trans. Power Syst.*, vol. 6, no. 3, pp. 914-921, 1991.

[33] T. Athay, R. Podmore, and S. Virmani, "A practical method for the direct analysis of transient stability," *IEEE Trans. Power Appar. Syst.*, vol. PAS-98, no. 2, pp. 573-584, 1979.

[34] J. H. Chow, *Power System Coherency and Model Reduction*. New York: Springer, 2013.
[35] J. Lara, J. Ramirez, and F. Macilla-David, "Allocation of PMU for power system-wide inertial frequency response estimation," *IET Gener. Transm. Distrib.*, vol. 11, no. 11, pp. 2902-2911, 2017.